

#### **Thermally Accelerated Curing of Platinum-Catalyzed Elastomers**

Te Faye Yap,<sup>1</sup> Anoop Rajappan,<sup>1</sup> Marquise D. Bell,<sup>1</sup> Rawand M. Rasheed,<sup>1</sup> Colter J. Decker,<sup>1</sup> and Daniel J. Preston<sup>1,\*</sup>

<sup>1</sup>Department of Mechanical Engineering, Rice University, Houston, Texas 77005, USA \*Correspondence: djp@rice.edu

#### **SUMMARY**

Silicone elastomers exhibit extraordinary compliance, positioning them as a material of choice for soft robots and devices. To accelerate curing times of platinum-catalyzed silicone elastomers, researchers have employed elevated temperatures; however, knowledge of the requisite duration for curing at a given temperature has remained limited to specific elastomers and relied primarily on empirical trends. This work presents an analytical model based on an Arrhenius framework coupled with data from thermo-rheological experiments to provide guidelines for suitable curing conditions for commercially available addition-cured platinum-catalyzed silicone elastomers. The curing reaction exhibits self-similarity upon normalizing to a dimensionless reaction coordinate, allowing quantification of the extent of curing under arbitrary time-varying thermal conditions. Mechanical testing revealed no significant changes in properties or performance as a result of thermally accelerated curing. With this framework, higher throughput of elastomeric components can be achieved and the design space for elastomer-based manufacturing can be developed beyond conventional casting.

Silicone; Temperature; Curing; Reaction Kinetics; Soft Robotics; Arrhenius Relationship

### CellPress

### Cell Reports Physical Science

#### INTRODUCTION

Silicone elastomers exhibit properties that make them an attractive class of materials for a variety of applications, for example (i) biocompatibility and softness for medical devices, implants, and prosthetics, 1,2 (ii) liquid-like properties (prior to curing) for painting or molding prosthetic makeup,<sup>3</sup> (iii) viscoelastic behavior that dampens vibrations for use as shock absorbers,4 (iv) low surface energy to create superhydrophobic surfaces and coatings that prevent dehydration, 5,6 (v) high temperature resistance for cookware, 7 and (vi) high dielectric strength for electrical insulation.<sup>8</sup> The versatility of silicone elastomers has also facilitated the growth of the field of soft robotics in which traditional rigid robotic components are progressively being supplemented or replaced with softer counterparts.<sup>9,10</sup> For instance, over the past decade, more than half of the soft robotic components developed were made from elastomers. 11 The embodied intelligence imparted by the mechanical compliance of elastomers reduces the complexity and number of control parameters required while allowing a soft robot to interact safely with delicate environments and conform to irregular objects. 9,12-14 Platinum-catalyzed addition-cured silicones represent the most commonly used elastomers in soft robotics, owing to their ease of use, commercial availability, and wide range of mechanical properties. 15-17 These addition-cured silicone elastomers are typically sold as two-part systems, one containing the platinum catalyst and the other the crosslinking agent (Figure 1). The two components start out as viscoelastic liquids which, after mixing, undergo crosslinking to form a network with no reaction byproducts (Figure 1B).7 The formation of crosslinks transforms the viscoelastic mixture into a solid rubber over a period of time known as the cure time, but the initial fluid state of the silicone prepolymer allows it to flow and conform to intricate mold geometries, a behavior that can be leveraged for casting complex components. 18-20

Elastomer-based robotic components, such as the pneumatic network (pneu-net) actuator, are usually fabricated by pouring the prepolymer into a 3D-printed negative mold.<sup>21,22</sup> During the casting step, the elastomer must be left inside the mold until it cures,

rendering the mold temporarily unavailable. After a component has fully cured, subsequent steps, such as assembling multiple components into assemblies or adding a fluidic connection for pressure-driven actuation, are performed to produce a finished device. Printing the mold typically consumes the most time of each of these individual tasks, and therefore limits the fabrication speed of one-off components;<sup>22</sup> however, as the number of components fabricated with a given mold increases, the curing step dominates the bulk of the fabrication time when performed at room temperature (Figure 1A).

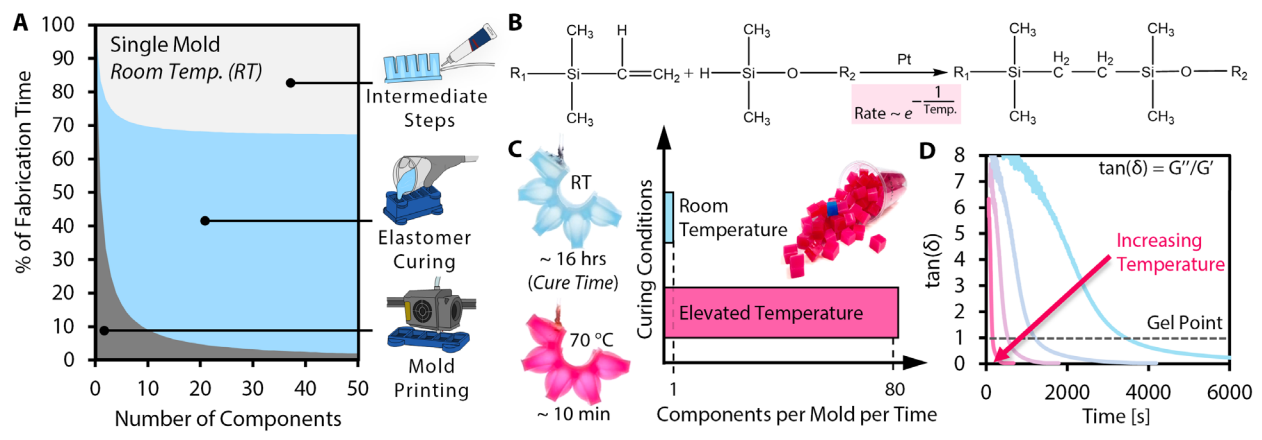


Figure 1. Thermally accelerated curing of platinum-catalyzed silicone elastomers

- (A) Typical method of fabricating soft actuators consists of casting the elastomer in a negative mold. The time required to create a single component consists of mold printing (which typically demands 50% of the total fabrication time), elastomer casting and curing (33%), and any intermediate steps to assemble and complete the final actuator (17%). As the number of casted components increases, however, the bulk of the fabrication time is dominated by curing (> 60%) if the same mold is used repeatedly.
- (B) The curing chemical reaction of platinum-catalyzed addition-cured silicone elastomers exhibits a rate of crosslinking with an exponential dependence on temperature.
- (C) Elevated temperatures are used to increase the rate of curing for platinum-catalyzed elastomers, leading to faster fabrication of soft actuators and greater production efficiency (up to two orders of magnitude more elastomeric components per time compared to curing at room temperature).
- (D) We quantitatively show that increasing temperature decreases the gel time, which is characterized as the time at which the loss tangent  $tan(\delta)$  equals 1, where  $tan(\delta)$  is defined as the ratio of the loss modulus (G") to the storage modulus (G').

#### **⊘** CellPress

### Cell Reports Physical Science

Researchers have observed that temperature can be used to speed up or slow down the time required to cure a component. Elevated temperatures have been used to reduce fabrication time by heating an elastomer-filled mold to accelerate the curing process. 16,17,21,23–27 Conversely, cooling the uncured elastomer mixture will delay the curing process and thereby prolong the "pot life" of the elastomer if more processing time is desired or to eliminate the need to prepare freshly mixed batches of elastomer for use in secondary post-curing steps. 15,21,25,26 The temperature and duration for curing, however, are often determined empirically based on trial and error without a mechanistic understanding of the reaction kinetics. Without guidelines, this approach can result in exposing a component to heat for longer than necessary and subsequently over-curing (and thus decreasing the adhesion between components during assembly of multicomponent devices) while also wasting energy during excess furnace dwell time; meanwhile, for cooling, it can result in uncertainty in the pot life during storage of uncured prepolymer, leading to failed attempts at casting.

To better understand this process, prior research has indicated that the rate of the curing reaction for hydrogels (such as gelatin), epoxies, and silicones exhibits an Arrhenius-like dependence on temperature;<sup>28–33</sup> however, in the case of elastomers, the quantitative analysis of how temperature affects the curing timescale has been limited to specific silicones, such as Sylgard 184,<sup>34</sup> and there is a need to characterize a broader range of commonly used, commercially available silicone elastomers to advance the field of soft robotics and other applications.<sup>24,31,35,36</sup> Furthermore, state-of-the-art models for the crosslinking kinetics of thermoset elastomers involve the superposition of multiple Arrhenius-type rate terms, introducing as many as nine free parameters or temperature-dependent exponents that must be determined by fitting to data obtained from differential scanning calorimetry (DSC) during curing.<sup>35</sup> Despite the specificity provided by such models, they do not provide any information on the mechanical properties of the elastomer during curing (which is crucial for material processing), and are not practical for high-level predictions of curing times; the application of these models becomes



especially complex when accounting for spatiotemporal variations in temperature. Moreover, an important consideration when selecting elastomers for fabricating soft robots is their mechanical properties after curing, which dictate the performance of the finished component. Prior work that employed elevated temperatures to accelerate the curing process did not investigate the effect of curing temperature (relative to curing at room temperature) on mechanical properties such as tensile strength and extensibility, which could be critical to the overall performance of the cured component. 16,21,23,37,38

In this work, we explore the temperature-dependent kinetics of crosslinking for a total of six commercially available elastomers from two of the most commonly used series of platinum-catalyzed silicone elastomers in the field of soft robotics, both of which are produced by Smooth-On: (i) Ecoflex 00-10, (ii) Ecoflex 00-30, (iii) Ecoflex 00-50, (iv) Dragon Skin 10 NV, (v) Dragon Skin 10 Medium, and (vi) Dragon Skin 30. We applied a thermo-rheological approach similar to prior work on gelation to characterize the curing process (Figure 1D). We used a kinetic model based on an Arrhenius framework in combination with data from small amplitude oscillatory shear (SAOS) tests to determine parameters specific to the curing chemistry of each elastomer (i.e., activation energy and frequency factor) to describe the crosslinking reaction underpinning elastomer curing, eliminating any guesswork required to determine the time and temperature for curing. The model quantitatively shows that by curing these slow-cure elastomers at temperatures easily achieved in low-cost ovens (e.g., 60-70 °C), cure times can be reduced by more than two orders of magnitude as compared to curing at room temperature (RT) (e.g., Dragon Skin 30, 16 h cure time at room temperature as stated by the manufacturer). We describe how this reduction in curing time results in significantly improved throughput, enabling rapid production of many components using a single mold (Figure 1C) while minimizing wasted energy resulting from heating components longer than required for curing. We also highlight that the crosslinking reaction exhibits temperature-independent self-similarity for these commercially available silicone elastomers, corroborated by superposition of experimentally measured dynamic moduli normalized by a characteristic



timescale based on the reaction coordinate. We demonstrate the use of the resulting self-similar "reduced curves" to track the extent of crosslinking and the dynamic moduli for an elastomer exposed to arbitrary heating conditions (i.e., any scalar field of temperature varying in both time and space) via the dimensionless reaction coordinate. To investigate whether differences in mechanical properties and performance arise as a consequence of thermally accelerated curing, we performed mechanical tests on elastomers cured at a range of temperatures, and we observed that elevated temperatures do not alter either the fundamental mechanical properties (e.g., elastic modulus and failure strength) of elastomers or the performance of an elastomeric pneu-net actuator, supporting the feasibility of using heat to modulate or accelerate the curing of elastomers.

#### **RESULTS**

#### Measuring gelation kinetics via mechanical spectroscopy

We performed small amplitude oscillatory shear (SAOS) tests using an ARES G2 rheometer to track the evolution of dynamic moduli (i.e., the storage modulus, G', and the loss modulus, G") of silicone elastomers during isothermal curing. The temperature, T, of the geometry was kept constant (within ± 0.1°C) using a Peltier module. A cone-and-plate geometry was used to perform the SAOS test at an angular frequency of 10 rad/s (or 1.6 Hz) and 0.25 % strain amplitude (see Supplemental Information, Figure S1, for more details). We dispensed 1 mL of each component ("part A" and "part B") for each elastomer sample in a weighing boat and manually stirred the mixture for ~1 minute (duration and method of mixing are shown in Figure S3 and S11 to have no effect on the overall properties of the samples). The prepolymer was then poured onto the geometry that had been preheated to the setpoint temperature (Figure S2). From the SAOS results, we inferred a characteristic timescale for crosslinking from the gel point, a method often used when studying curing behavior. 18,20,24,32,39 For simplicity, we employed a commonly used characterization of the gel point, and according to the ASTM 4473 standard, as the time at which the loss tangent,  $\tan \delta = G'' / G'$ , reaches unity (also known as the crossover point);<sup>32,39</sup> beyond the gel point, the storage modulus of the elastomer exceeds its loss



modulus, indicating a more solid-like behavior. Because elevated temperatures will expedite the curing process, we quantified our experiment "setup time," i.e., the time elapsed between pouring the elastomer on the pre-heated test geometry and the start of the SAOS measurement (see Supplemental Information), which we added to the gelation time obtained from the data to determine the actual gelation time,  $t_{\rm gel}$  (setup time at room temperature was neglected). We performed experiments for six elastomers: (i) Ecoflex 00-10, (ii) Ecoflex 00-30, (iii) Ecoflex 00-50, (iv) Dragon Skin10 NV, (v) Dragon Skin 10 Medium, and (vi) Dragon Skin 30, with three measurements taken at each of four distinct temperatures (a total of 72 thermo-rheological experiments), and plotted the dynamic moduli for representative experiments at each temperature in Figure 2A.

#### Determining the activation energy and frequency factor

The temperature dependence of polymer gelation has been shown to exhibit Arrhenius-like behavior,  $^{28-32}$  mirroring other temperature-dependent phenomena such as diffusion, creep, and even the inactivation of viruses. Using the gelation time  $t_{gel}$  at each temperature T obtained from SAOS experiments, we can plot the data according to the linearized Arrhenius equation (Figure 2B):

$$\ln(t_{\text{gel}}) = \frac{E_a}{RT} - \ln(A)$$
 (Equation 1)

where R is the gas constant,  $E_a$  is the activation energy, and A is a constant proportional to the Arrhenius frequency factor. The values for  $E_a$  and A for each elastomer were determined by equating the slope of the best fit line to  $E_a/R$  and the intercept to In(A) (Figure S4, Table S3).



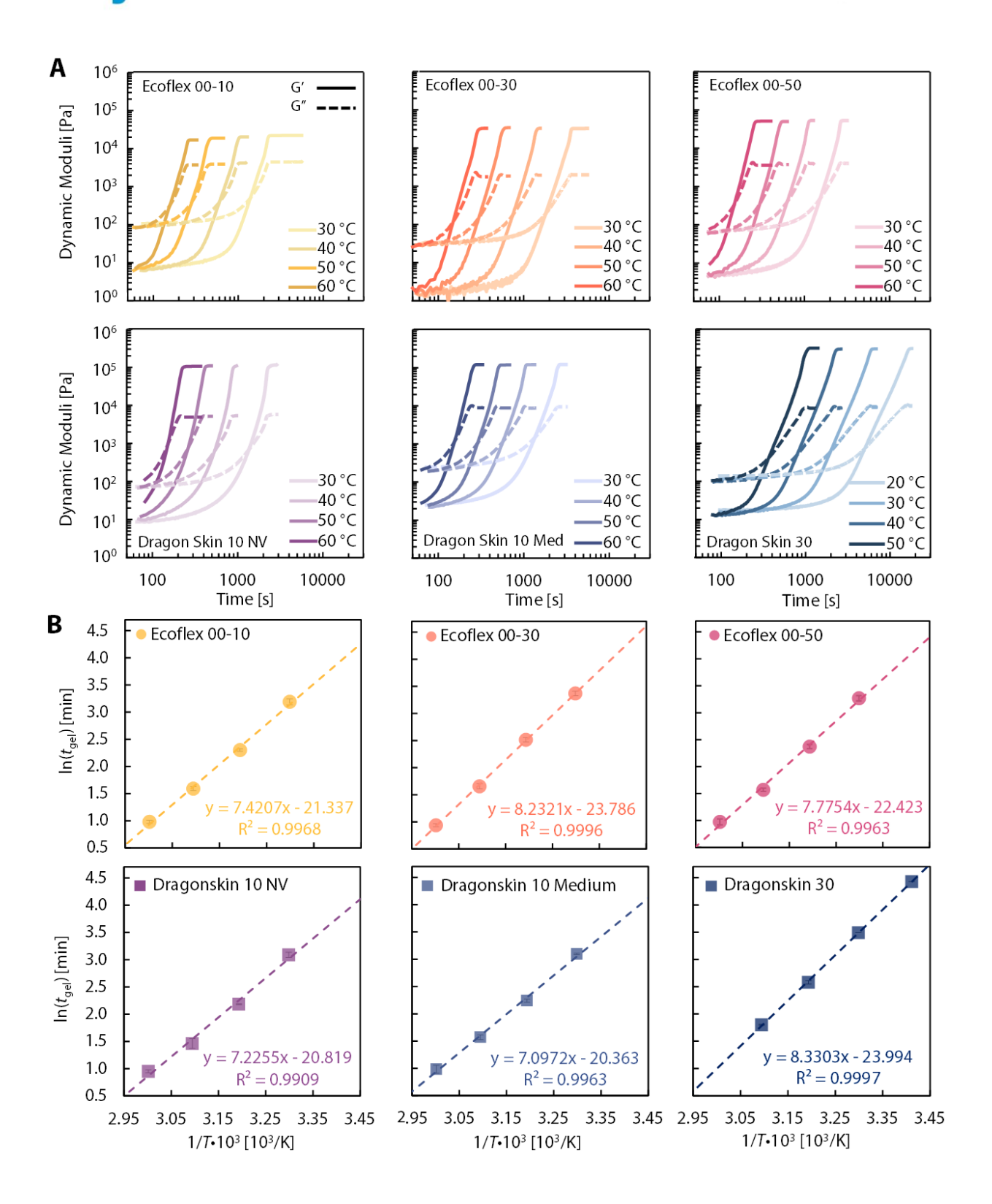




### Figure 2. Dynamic moduli curves and corresponding gelation times at each temperature plotted according to the linearized Arrhenius equation

- (A) Dynamic moduli (storage modulus denoted with solid lines and loss modulus denoted with dashed lines) obtained from small amplitude oscillatory shear (SAOS) experiments for six elastomers. Experimental setup time was recorded and added to offset the time axis to account for sample crosslinking when in contact with the preheated test geometry before the start of the experiment. The point at which the storage and loss moduli intersect is taken as the gelation time,  $t_{\rm gel}$ , for each temperature.
- (B) The gelation time at each temperature was plotted according to the linearized Arrhenius equation, and the values of slopes and intercepts from best fit lines yielded the activation energy,  $E_a$ , and the frequency factor, A. All best fit lines had a coefficient of determination  $R^2$  greater than 0.99. Error bars represent the standard deviation across three experiments.

We found that the value of  $\ln(A)$  varies linearly with  $E_a$  across the range of elastomers tested (Figure 3A), indicating that the crosslinking of these silicones follows the Meyer-Neldel rule, which has been observed in other phenomena such as virus inactivation, ion diffusion, fouling, and electrical conductivity of solids. An a result of this Meyer-Neldel relationship, the slope of the best fit curve in Figure 3A can be used to determine the isokinetic temperature—i.e., the temperature at which the crosslinking reaction proceeds at the same rate for all silicone elastomers—for which all the elastomers studied in this work exhibit approximately the same gelation time, which we determined to be 65.5°C (Figure 3B). The values for  $E_a$  and  $\ln(A)$  determined experimentally for each elastomer are substituted into Equation 1 to predict the gelation time as a continuous function of temperature (Figure 3C,D, Figure S5).

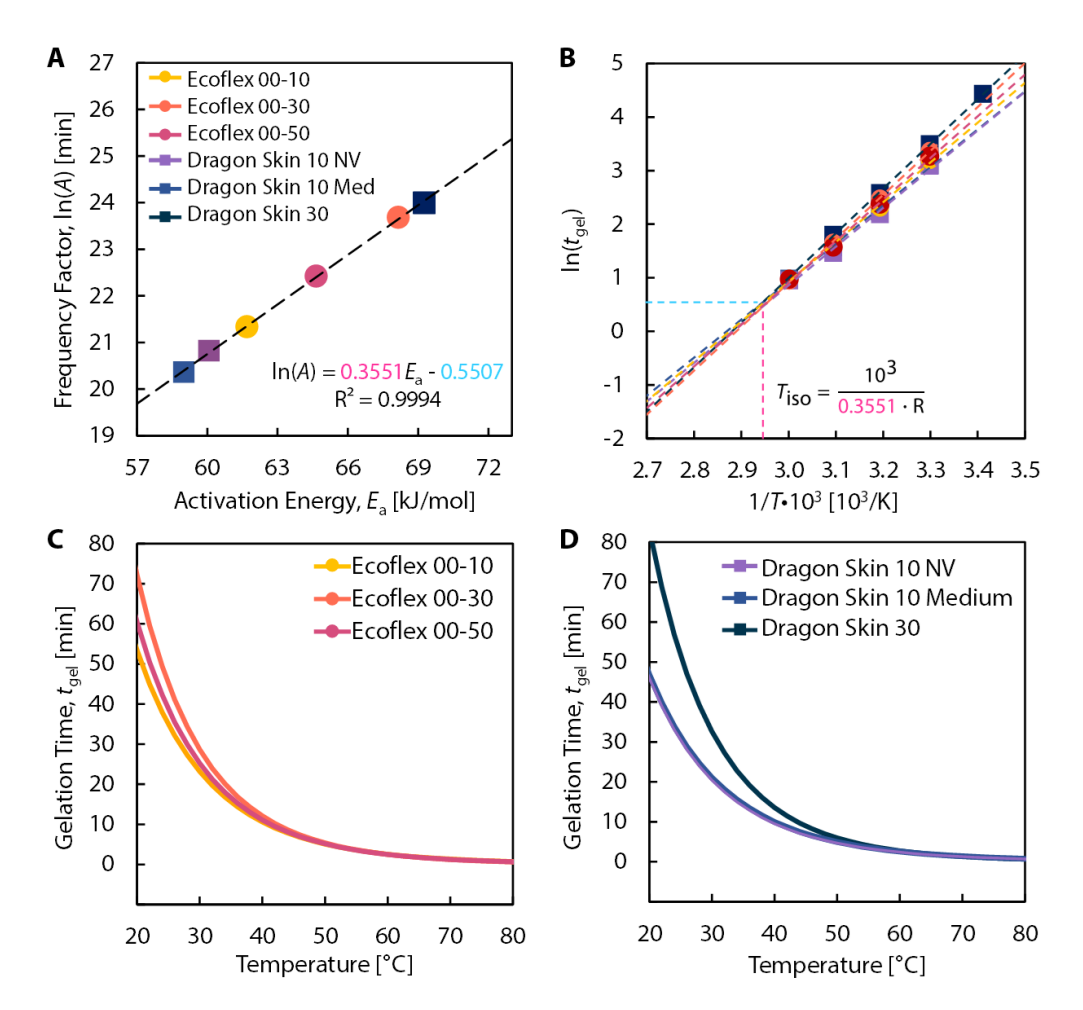


Figure 3. Prediction of gelation time as a function of temperature

- (A)  $E_a$  and In(A) determined for all six elastomers studied in this work; the linear fit shows that the crosslinking reaction follows the Meyer-Neldel rule.
- (B) The isokinetic temperature can be determined from the slope of  $E_a$  vs In(A) and is corroborated by the concurrent intersection of the best fit lines plotted according to the linearized Arrhenius equation for all elastomers.
- (C and D) The predicted gelation time for each elastomer as a function of temperature, determined using  $E_a$  and In(A) in Equation 1, is shown for (C) Ecoflex and (D) Dragon Skin families of elastomers.

#### Modeling non-isothermal curing with self-similar curing kinetics

The predicted gelation time in Figure 3B assumes isothermal curing, i.e., the elastomeric component being cured experiences a constant and uniform temperature. However, in reality, components with a significant thermal mass will require a non-negligible heating



duration to achieve an elevated temperature via natural or forced convection. To expand the capabilities of our modeling framework, we predict the time required to cure an elastomeric component in a mold that has a transient temperature profile. We first describe the temperature evolution of the component that is being heated in an oven at ~60 °C using the lumped capacitance equation:

$$T(t) = (T_i - T_o) \exp\left(-\frac{hA_s}{\rho C_p V}t\right) + T_o$$
 (Equation 2)

where  $T_0$  is the setpoint temperature of the oven,  $T_1$  is the initial temperature of the elastomer in the mold, h is the convective heat transfer coefficient of the surrounding air in the oven,  $A_s$  and V are the surface area and volume of the component being cured,  $c_p$  is the specific heat capacity, and  $\rho$  is the density of the elastomer. The lumped capacitance assumption—i.e., a uniform temperature throughout the material—is valid because the geometry we used satisfies the low Biot number (Bi << 1) requirement (details in Supplemental Information, Section 2). We plot the temperature profile predicted by the lumped capacitance model in Figure 4A, including a constant value of room temperature for 5 minutes initially to account for the mixing and degassing time prior to loading the elastomer into the oven. We recorded the real-time temperature inside the oven as well as the temperature of the component being cured in the mold as a function of time using a pair of thermocouples. Aside from discrepancies due to the temperature fluctuations of the oven itself, the lumped capacitance model captures the transient temperature response with reasonable accuracy.

#### **CellPress**

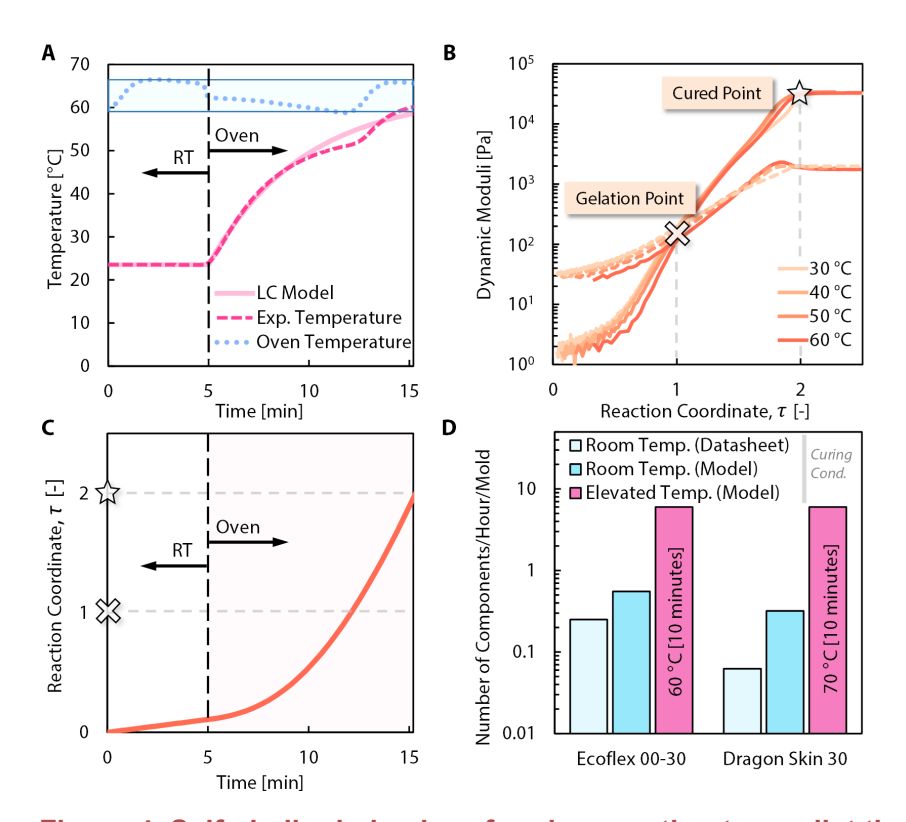


Figure 4. Self-similar behavior of curing reaction to predict the cure extent for timevarying temperature profiles

- (A) The temperature profile determined using the lumped capacitance (LC) model with an initial 5 minute setup time at room temperature (solid pink). The temperature profile was obtained experimentally with a thermocouple inside an elastomeric component (dotted pink) while being cured in an oven at an elevated temperature, shown alongside the real-time temperature of the oven (blue).
- (B) The dynamic moduli of the elastomer (Ecoflex 00-30) collapse onto a reduced curve after the time axis is normalized by the gelation time. From the reduced curve, we were able to extract the reaction coordinate,  $\tau$ , at which the elastomer has cured fully. From this self-similar curve, the curing point for Ecoflex 00-30 occurs at  $\tau \approx 2$ , or double the gelation time.
- (C) The reaction coordinate  $\tau$  as a function of time was determined numerically using Equation 4 based on the temperature profile of the LC model shown in (A). When the reaction coordinate reaches 2, the elastomer has attained its maximum shear modulus and has fully cured.
- (D) Based on this reduced curing time, we are able to create more components per mold over a fixed duration of time using elevated temperatures. We show that curing at 60 °C and 70 °C yields 24× and 96× the number of components (for the specific geometry used here), respectively, over the same time compared to curing at room temperature (as specified in the datasheet) for Ecoflex 00-30 and Dragon Skin 30. When compared to the curing time at room temperature determined from our model, we predict an order of magnitude increase in throughput when curing with elevated temperatures.



We further used the gelation time for each elastomer at different temperatures to rescale the time axis,  $\tau = t/t_{\rm gel}$ , for each set of transient curing data obtained from SAOS timesweeps. 46,47 Upon rescaling, the storage and loss moduli curves at each temperature for a given elastomer collapse onto a single reduced curve (Figure 4B, Figure S6), exhibiting self-similar behavior and illustrating that the dimensionless shapes of the dynamic moduli curves do not change with temperature. The nondimensionalized time  $\tau$  can be interpreted as a reaction coordinate that increases monotonically as crosslinking progresses, and its value indicates the transient state of the elastomer as it is curing. When  $\tau = 1$ , the elastomer has reached its gel point (denoted by a 'cross'), and we identify the cure point as the point at which the storage modulus reaches a plateau region (denoted by a 'star'). The value of T at the cure point varies for each elastomer (see Supplemental Information). In Figure 4B, we show the collapsed reduced curve for Ecoflex 00-30; the value of τ at which the elastomer has cured is approximately 2, indicating that the cure time is double the gelation time for this elastomer. Self-similar curves for all the elastomers characterized in this work and their cure point T values are provided in the Supplemental Information, Section 3.

To incorporate the effect of a time-varying temperature when predicting the elastomer cure rate, we combined the lumped capacitance model (Equation 2) with the temperature-dependent rate law in Equation 1. Adapting our definition of the reaction coordinate for transient temperatures, we obtain:

$$\frac{d\tau}{dt} = Ae^{-\frac{E_a}{RT(t)}}$$
 (Equation 3)

which, in integral form, reads:

$$\tau(t) = \int_{t_0}^{t} Ae^{-\frac{E_a}{RT(t)}} dt + \tau_0$$
 (Equation 4)

#### **CellPress**

### Cell Reports Physical Science

The integral on the right-hand side of the equation is computed numerically using a fourth order Runge-Kutta (Dormand-Prince) method, where  $\tau_0 = 0$  at t = 0. Figure 4C shows the reaction coordinate as a function of time corresponding to the temperature profile in Figure 4A, from which we determined the gelation and cure points of the elastomer. For a nominal oven temperature of  $T \approx 60$  °C, the elastomer inside the mold was shown to cure within 10 minutes, which is 24× faster than the 4 h cure time required for Ecoflex 00-30 at room temperature as specified by the manufacturer. We also show for Dragon Skin 30, which has a longer curing time of 16 hours (according to the datasheet), that a part can cure within 10 minutes at 70 °C, we achieve 96× faster than curing at room temperature (Figure 4D). Because the manufacturers follow different criteria for determining the curing time, we also compared the curing time at room temperature and elevated temperature predicted by our modeling framework, and we show an order of magnitude greater throughput for both elastomers when using elevated temperatures for curing. For the same duration, curing the part inside the oven therefore achieves a substantially higher throughput, by approximately two orders of magnitude, for a single mold for either elastomer. This accelerated curing decreases the number of molds that would otherwise be needed to fabricate a large number of parts within a specified timeframe.

We also verified our model with results in the literature obtained independently of our work (Figure 5). We compared our predicted results with experimental measurements by Xie et al., who recorded the dynamic moduli of Ecoflex 00-50 subjected to temperature ramps of different rates.<sup>35</sup> As a reference, we used the reduced curve for Ecoflex 00-50 that we determined by averaging the dynamic moduli across the four temperatures at which we performed SAOS tests (the methodology for averaging the reduced curve is described in the Supplemental Information, Section 3); the ranges of storage and loss moduli determined from SAOS experiments at four temperatures are denoted by the light pink shaded regions (Figure 5A), and the curing point occurs at τ ≈ 1.8. Using Equation 4, we computed the evolution of τ as a function of time for a



temperature ramp of 10 °C per minute starting from room temperature, corresponding to the protocol adopted by Xie et al. for their rheological measurements.

As a preliminary verification, we estimated the sample temperature corresponding to the gel point ( $\tau$  = 1) and cure point ( $\tau$  = 1.8) during their experiment, as shown by the dotted lines in Figure 5B.

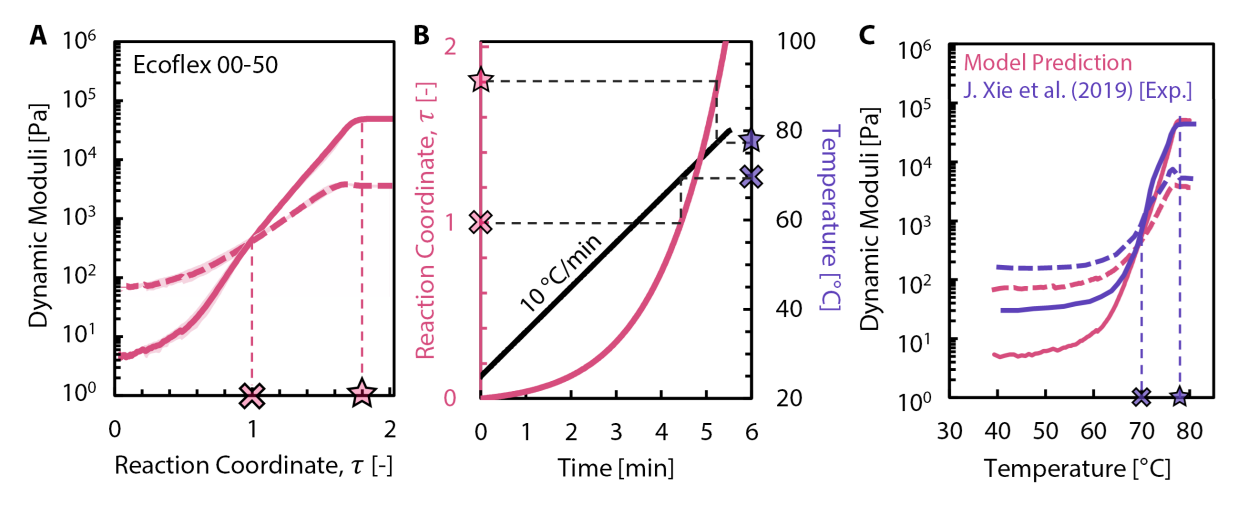


Figure 5. Comparison of the modeling framework with independent results

- (A) The reduced curve for Ecoflex 00-50 generated by averaging the normalized data obtained at four temperatures. The shaded region represents the min and max range of dynamic moduli values.
- (B) The black curve indicates the temperature profile with a 10 °C/min ramp as performed in prior work by Xie et al., and the pink curve indicates the corresponding reaction coordinate determined using Equation 4. Using this temperature profile, we determined the temperature at which Ecoflex 00-50 reaches its gel and cure points by first relating the reaction coordinate at  $\tau$  = 1 and 1.8 to the corresponding times, and then identifying the corresponding temperatures at those times. The temperatures at which the elastomer reaches the gel and cure points are denoted with a cross and star, respectively, on the temperature axis.
- (C) Using the reduced curve in (A), we estimated the dynamic moduli using the reaction coordinate  $\tau$  predicted by our model. Values predicted by our model (pink curves) show good agreement with the experimental data reported by Xie et al. (purple curves) in the region beyond the crossover point. The temperatures corresponding to the gel and cure points are again indicated as in (B) on the x-axis.



Our model predicts that the gel and cure point occur when the temperature reaches 69 °C and 77 °C (indicated by the 'cross' and the 'star' in Figure 5C, respectively, in good agreement with the experimental values of 70 °C and 78 °C reported by Xie et al., thus providing independent validation of our model's capability to predict the curing behavior of elastomers. We also applied our modeling framework to back-calculate the evolution of dynamic moduli during crosslinking under non-isothermal curing conditions. We used the reduced curve from Figure 5A and related each T value to a corresponding loss and storage modulus (more details in Supplemental Information, Section 3). In Figure 5C, we show the dynamic moduli that we predicted (pink) against experimental data obtained by Xie et al. (purple) as a function of temperature for their dynamic rheological measurement at a heating rate of 10 °C per minute; the temperature axis can also be converted to a time axis using the known, constant heating rate. We repeated this analysis for their experiment performed at a heating rate of 1°C per minute, which also showed good agreement with our prediction (Figure S7). Our model is thus able to extrapolate the kinetics of crosslinking of silicone elastomers based on experimental data obtained at a few temperatures, enabling the prediction of cure times and curing behavior not just for isothermal curing conditions, but also for more complex timevarying temperature profiles.

#### Effect of elevated temperature curing on mechanical properties and performance

Although elevated temperatures have been employed in prior work to decrease the fabrication time of soft robotic components, the effect of accelerated curing, if any, on the mechanical properties of the cured elastomer has not been conclusively investigated in the literature.<sup>37,48,49</sup> This analysis is important because the mechanical behavior of the elastomer ultimately dictates the behavior of the resulting soft device, which in the case of soft robotics, for example, could be an actuator. Although mechanical testing has been performed in prior studies on some elastomers after curing at elevated temperatures, these results have not been compared with components cured at room temperature.<sup>37</sup>



To fill this gap, we investigated the mechanical properties of elastomers cured at elevated temperatures and compared them against those of elastomers cured at room temperature as a baseline. We performed tensile tests on dog bone samples (as specified in the ASTM D412 standard for rubbers) on a universal testing machine (see Supplemental Information, Section 4).<sup>48–50</sup> We report the tensile test data performed at a rate of 500 mm/min for Dragon Skin 30 and Ecoflex 00-30 elastomers, cured at 70 °C and 60 °C, respectively, in Figure 6. Tensile test data for Dragon Skin 30 and Ecoflex 00-30 were obtained at a lower strain rate (100 mm/min), and showed no difference in the mechanical behavior (Figure S10). Tensile test experiments for all other elastomers studied in this work are provided in Figure S9. We also performed compression tests on cuboidal samples to investigate the mechanical behavior of the same elastomers under compressive stresses. Results from these mechanical tests revealed no discernible difference in the response to tensile and compressive stresses between elastomer samples cured at elevated temperatures and those cured at room temperature (Figure 6 A-D).

For further comparison, we report the values of the Young's modulus, E, the maximum tensile stress,  $\sigma_{max}$ , and the maximum tensile strain,  $\varepsilon_{max}$ , of the elastomers obtained from three trials of tensile testing, and we compare the average values obtained experimentally to those supplied in the manufacturer's datasheet (Figure 6 E,F). The maximum tensile strain obtained directly from the crosshead displacement (solid bars) exhibits higher values relative to those reported in the manufacturer's datasheet. This discrepancy is attributed to deformation of the sample at the grips, which results in greater strain values than the actual strain occurring at the gauge length region. Using optical extensometry, we quantified the strain occurring locally at the gauge region, and the magnitude of the optically determined maximum strain (diagonally shaded bars) is comparable to the values reported in the datasheet. Our experimental results confirm that the temperature at which the elastomers were cured did not significantly alter the mechanical performance, and thermal modulation is therefore a viable strategy for controlling the rate





of curing with either elevated temperatures to fabricate more components per mold per time or cold temperatures to delay curing for storage or to prolong the working time of the prepolymer (Figure S14) without affecting the overall mechanical properties.

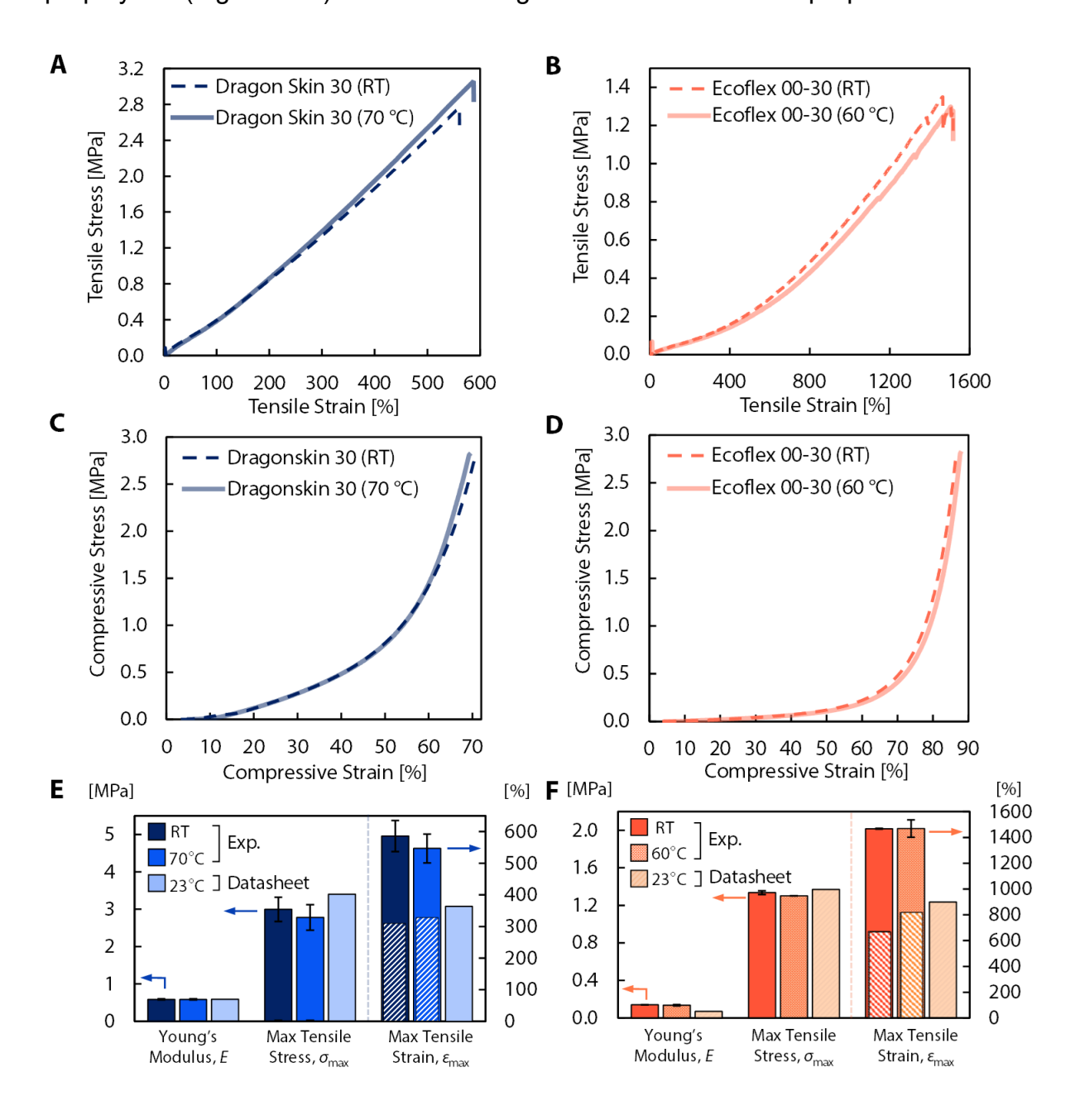




#### Figure 6. The effect of elevated temperature curing on mechanical properties

(A and B) Tensile test results corresponding to the crosshead values for (A) Dragon Skin 30 and (B) Ecoflex 00-30 (performed on an ASTM D412 dog bone sample) were obtained to compare the tensile performance when cured at room temperature to the performance when cured at elevated temperatures, with no significant difference in performance between the two cases.

(C and D) Compression test results show no significant difference in mechanical behavior or performance and follow the expected trend for elastomeric materials.

(E and F) Young's modulus, maximum tensile stress, and maximum tensile strain values were compared across three experiments for (E) Dragon Skin 30 and (F) Ecoflex 00-30 cured at room temperature and elevated temperatures, shown alongside values obtained for curing at 23 °C from the manufacturer's datasheet. Maximum tensile strain values determined using the crosshead displacement are indicated with solid bars, while values obtained with optical extensometry are indicated with bars shaded with diagonal lines to account for discrepancies in crosshead strain measurements that arise due to deformation of the samples near the grips. Error bars represent the standard deviation across three trials.

As a further demonstration of accelerated curing of soft robotic components at elevated temperatures, we fabricated pneumatic network (pneu-net) actuators at both room temperature and elevated temperatures and evaluated their performance (fabrication details in Supplemental Information, Figure S12). We recorded the bending profile of the pneu-nets upon quasi-static pressurization with compressed air (Figure 7A), and we determined the curvature κ (inverse of the bending radius) as a function of actuation pressure. In Figure 7B and C, we compare the experimentally measured curvature of the pneu-net actuators made from Ecoflex 00-30 and Dragon Skin 30 elastomers at various pressures; the deformation was identical for actuators cured at room temperature and at elevated temperatures (Movie S1). This demonstration highlights that accelerated curing at elevated temperatures decreases fabrication time while retaining the anticipated performance of the soft actuator.

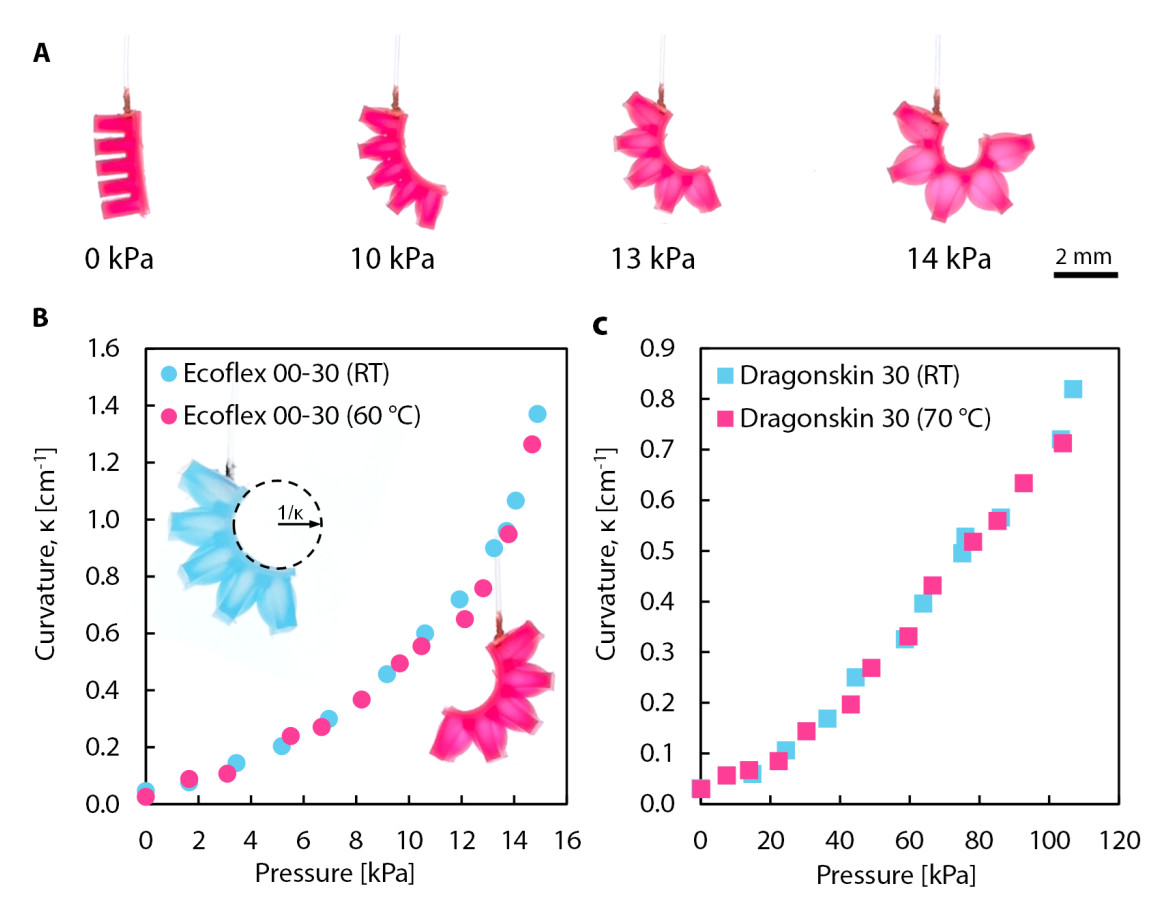


Figure 7. Investigating the effect of elevated temperature curing on mechanical performance of pneu-net actuators

(A) Time lapse images of an Ecoflex 00-30 pneu-net actuator being quasi-statically pressurized. (B and C) The curvature of the pneu-net is shown as a function of pressure for both (B) Ecoflex 00-30 and (C) Dragon Skin 30 cured at room temperature and at elevated temperatures.

#### **DISCUSSION**

We showed using tensile and compression tests that the mechanical properties of the material do not vary significantly within the range of curing temperatures that we tested; however, extreme temperatures (close to the recommended maximum and minimum working temperatures for the elastomers which corresponds to -53°C to 232°C according to the manufacturer's datasheet) could potentially affect the mechanical properties of the final cured component or cause chemical degradation. Future studies can identify the full temperature range for curing that will not significantly affect the performance, as well as

### CelPress

### Cell Reports Physical Science

temperatures that will alter the mechanical properties such that the mechanical response of the elastomer can be spatially programmed with temperature to create functional, monolithic actuators without any need for a secondary adhesion step, decreasing the risk of assembly failure at the joints. For instance, mechanical properties that can be spatially tuned with extreme temperatures could potentially allow for local changes in stiffness (or Young's modulus) that would allow increased or decreased deformation at a given actuation pressure. Additionally, the effect of temperature on viscosity should be accounted for, especially when modeling a flow-mediated process where the flowing prepolymer is simultaneously undergoing curing. 18–20,52 We included a plot of the complex viscosity as a function of reaction coordinate, and showed that higher temperatures will result in a lower viscosity of the prepolymer (Figure S13). We also note that the shelf life or period after opening (PAO) of the elastomers, as well as the presence of thinners, retarders, contaminants, or inhibitors, could also influence the gelation time; all experiments conducted in this work used fresh elastomer kits that were tested within a month of opening to limit the effect of PAO on the reaction kinetics.

The modeling framework proposed in this work enables prediction of the temperature-dependent curing of commercially available silicone elastomers commonly used for fabrication of soft robotic actuators. The approach used in this work can also be applied to differential scanning calorimetry (DSC) data as shown in prior studies in the literature. 28,29,34,35 In our work we use a mechanical rather than a calorimetric analysis of the progress of the curing reaction to determine the dynamic mechanical properties of the elastomer; However, the underlying physics of the crosslinking reaction obey the Arrhenius equation and should work for both methods. Based on the Arrhenius equation with only two physical parameters—namely, the activation energy and frequency factor—our model accurately predicts the crosslinking rate of silicone elastomers during curing, as validated by comparisons against rheological measurements performed here and reported previously in the literature. This understanding of the temperature-dependent curing reaction elucidates the time required to cure an elastomeric component at an



elevated temperature while reducing energy wastage that would be incurred by heating the component for longer than necessary. Furthermore, the reduced curves generated by nondimensionalizing the time coordinate to a reaction coordinate allow tracking of the evolution of dynamic moduli for complex, time-varying temperature profiles as an elastomer cures. Using this capability, the modeling framework can therefore be incorporated into the design space of additive manufacturing using off-the-shelf thermally curable elastomers, circumventing the need to modify the chemistry to be photopolymerizable for stereolithography (SLA) or digital light processing (DLP) printing, and taking advantage of the unmodified properties of these commercial elastomers. 53,54 The parameters for vat photopolymerization and extrusion-based 3D printing of thermally curable elastomers can be fine-tuned based on the fundamental understanding of the temperature dependence of the extent of curing presented in this work to optimize the printed component and promote better layer-by-layer adhesion.<sup>24,36,53,55-57</sup> Although mainly demonstrated for platinum-catalyzed, addition-cured silicone elastomers, the thermo-rheological modeling framework may be extended to other commonly used thermosets that exhibit temperature-dependent crosslinking, such as polyepoxides, natural rubbers, and polyurethanes. Ultimately, in addition to guiding existing fabrication methods, the ability to thermally control curing will generate avenues for complex manufacturing techniques extending beyond casting and molding, achieved through precise spatiotemporal control over temperature.

#### **EXPERIMENTAL PROCEDURES**

#### **Resource Availability**

#### Lead Contact

Further information and requests for resources and reagents should be directed to and will be fulfilled by the Lead Contact, Daniel J. Preston (dip@rice.edu).

#### Materials Availability

This study did not generate any new materials.

### **⊘** CellPress

### Cell Reports Physical Science

#### Data and Code Availability

All data needed to evaluate the conclusions in the paper are present in the paper and/or the supplemental information. Additional data related to this paper may be requested from the authors. This paper does not report any original code or algorithms.

#### **Mechanical Spectroscopy**

Small amplitude oscillatory shear (SAOS) experiments were performed on an ARES G2 rheometer using a cone and plate fixture (25 mm, 0.1 rad). A Peltier system was used to modulate and maintain the temperature of the bottom plate. The tests were performed at a frequency of 10 rad/s and strain amplitude of 0.25% (selected because it was within the linear viscoelastic regime). The prepolymer was prepared by dispensing 1 mL each of part A and part B into a weighing boat and manually mixing for ~ 1 minute (see Supplemental Information for more details, Figures S3 and S11). Prepolymers with viscosities greater than 20,000 cPs were degassed for 5 minutes prior to loading onto the bottom plate. The setup time was recorded as the time between loading the sample onto the bottom plate and starting the experiment

#### **Mechanical Testing**

A universal testing machine (Instron, 68SC-2) was used to perform tension and compression tests on the elastomers cured at different temperatures. Each tensile test was performed on an elastomer sample with a dog bone geometry (made according to the ASTM-D412 standard) at a strain rate of 500 mm/min. Tests were also performed at 100 mm/min to show that the stress-strain curves obtained in this work represent quasistatic behavior and are independent of strain rate (Figure S10).

#### **Mold Fabrication**

The negative molds for the pneumatic network actuator and dog bone tensile test were manufactured using a fused deposition modeling (FDM) additive manufacturing process. The molds were designed in a computer and A Creality CR10s Pro v2 FDM 3D printer



was used to manufacture the molds. The molds were printed from polylactic acid (PLA) filament at a print speed of 60 mm/s, nozzle temperature of 215 °C, and build plate temperature of 50 °C. Once the prints were completed, the molds were removed from the build plate.

#### **Temperature Measurement**

The real-time temperature measurements of the elastomer and the oven were obtained using 0.01-inch diameter fiberglass-insulated T-type thermocouples from Omega. Temperature data were processed using MATLAB with a NI-9212 DAQ.

#### SUPPLEMENTAL INFORMATION

Supplemental information can be found online at

Document S1. Supplemental Experimental Procedures, Figures S1–S15, and Tables S1–S3

Video S1. Comparison of pneu-net actuation

#### **ACKNOWLEDGMENTS**

T.F.Y. would like to thank Trevor J. Shimokusu for helpful discussions and feedback on the manuscript. This study used equipment maintained and administered by the Shared Equipment Authority at Rice University. This material is based upon work supported by the National Science Foundation under Grant No. CMMI-2144809. Any opinions, findings, and conclusions or recommendations expressed in this material are those of the authors and do not necessarily reflect the views of the National Science Foundation. A.R. acknowledges support from the Rice University Academy of Fellows. M.D.B. recognizes support from a NASA Space Technology Graduate Research Opportunity award (80NSSC21K1276) and a National GEM Consortium Fellowship. R.M.R. acknowledges support from the U.S. Department of Energy (DOE) Innovation in Buildings (IBUILD) fellowship. This research was supported in part by an appointment with the Energy Efficiency & Renewable Energy (EERE) Science, Technology and Policy Program



sponsored by the U.S. Department of Energy (DOE). This program is administered by the Oak Ridge Institute for Science and Education (ORISE) for the DOE. ORISE is managed by ORAU under DOE contract number DE-SC0014664. All opinions expressed in this paper are the author's and do not necessarily reflect the policies and views of DOE, ORAU, or ORISE.

#### **AUTHOR CONTRIBUTIONS**

Conceptualization, T.F.Y., A.R., and D.J.P.; Methodology, T.F.Y., A.R., and D.J.P.; Investigation, T.F.Y., A.R., M.D.B., R.M.R., C.J.D.; Visualization, T.F.Y, A.R.; Supervision, D.J.P.; Writing – Original Draft, T.F.Y, A.R., D.J.P.; Writing – Review & Editing, T.F.Y, A.R., M.D.B., R.M.R., C.J.D., D.J.P.

#### **DECLARATION OF INTERESTS**

The authors declare no competing interests.

#### References

- 1. Colas, A., and Curtis, J. (2004). Application of materials in medicine, biology, and artifical organs. In Biomaterials Science: An Introduction to Materials in Medicine (Elsevier), pp. 697–704.
- 2. MacCallum, N., Howell, C., Kim, P., Sun, D., Friedlander, R., Ranisau, J., Ahanotu, O., Lin, J.J., Vena, A., Hatton, B., et al. (2015). Liquid-Infused Silicone As a Biofouling-Free Medical Material. ACS Biomater. Sci. Eng. *1*, 43–51. 10.1021/ab5000578.
- 3. Smooth-On: Makeup FX https://www.smooth-on.com/applications/makeup-fx/.
- Rodriguez, N., Ruelas, S., Forien, J.-B., Dudukovic, N., DeOtte, J., Rodriguez, J., Moran, B., Lewicki, J.P., Duoss, E.B., and Oakdale, J.S. (2021). 3D Printing of High Viscosity Reinforced Silicone Elastomers. Polymers 13, 2239. 10.3390/polym13142239.
- 5. Wang, G., Li, A., Zhao, W., Xu, Z., Ma, Y., Zhang, F., Zhang, Y., Zhou, J., and He, Q. (2021). A Review on Fabrication Methods and Research Progress of Superhydrophobic Silicone Rubber Materials. Adv. Mater. Interfaces *8*, 2001460. 10.1002/admi.202001460.



- 6. Yuk, H., Zhang, T., Parada, G.A., Liu, X., and Zhao, X. (2016). Skin-inspired hydrogel–elastomer hybrids with robust interfaces and functional microstructures. Nat Commun *7*, 12028. 10.1038/ncomms12028.
- 7. Polmanteer, K.E. (1981). Current Perspectives on Silicone Rubber Technology. Rubber Chemistry and Technology *54*, 1051–1080. 10.5254/1.3535846.
- 8. Xu, S., Chen, Y., Hyun, N.P., Becker, K.P., and Wood, R.J. (2021). A dynamic electrically driven soft valve for control of soft hydraulic actuators. Proc. Natl. Acad. Sci. U.S.A. *118*, e2103198118. 10.1073/pnas.2103198118.
- 9. Rajappan, A., Jumet, B., and Preston, D.J. (2021). Pneumatic soft robots take a step toward autonomy. Sci. Robot. *6*, eabg6994. 10.1126/scirobotics.abg6994.
- Drotman, D., Jadhav, S., Sharp, D., Chan, C., and Tolley, M.T. (2021). Electronics-free pneumatic circuits for controlling soft-legged robots. Sci. Robot. 6, eaay2627. 10.1126/scirobotics.aay2627.
- 11. Jumet, B., Bell, M.D., Sanchez, V., and Preston, D.J. (2021). A Data-Driven Review of Soft Robotics. Advanced Intelligent Systems, 2100163. 10.1002/aisy.202100163.
- 12. Tauber, F., Desmulliez, M., Piccin, O., and Stokes, A.A. (2023). Perspective for soft robotics: the field's past and future. Bioinspir. Biomim. *18*, 035001. 10.1088/1748-3190/acbb48.
- 13. Laschi, C., and Mazzolai, B. (2016). Lessons from Animals and Plants: The Symbiosis of Morphological Computation and Soft Robotics. IEEE Robot. Automat. Mag. 23, 107–114. 10.1109/MRA.2016.2582726.
- 14. Whitesides, G.M. (2018). Soft Robotics. Angew. Chem. Int. Ed. *57*, 4258–4273. 10.1002/anie.201800907.
- 15. Preston, D.J., Rothemund, P., Jiang, H.J., Nemitz, M.P., Rawson, J., Suo, Z., and Whitesides, G.M. (2019). Digital logic for soft devices. Proc. Natl. Acad. Sci. U.S.A. *116*, 7750–7759. 10.1073/pnas.1820672116.
- 16. Paternò, L., Tortora, G., and Menciassi, A. (2018). Hybrid Soft–Rigid Actuators for Minimally Invasive Surgery. Soft Robotics *5*, 783–799. 10.1089/soro.2017.0140.
- 17. McCandless, M., Gerald, A., Carroll, A., Aihara, H., and Russo, S. (2021). A Soft Robotic Sleeve for Safer Colonoscopy Procedures. IEEE Robot. Autom. Lett. 6, 5292–5299. 10.1109/LRA.2021.3073651.



- 18. Jones, T.J., Jambon-Puillet, E., Marthelot, J., and Brun, P.-T. (2021). Bubble casting soft robotics. Nature *599*, 229–233. 10.1038/s41586-021-04029-6.
- 19. Becker, K.P., Chen, Y., and Wood, R.J. (2020). Mechanically Programmable Dip Molding of High Aspect Ratio Soft Actuator Arrays. Adv. Funct. Mater. *30*, 1908919. 10.1002/adfm.201908919.
- 20. Badaoui, M., Kresge, G., Ushay, C., Marthelot, J., and Brun, P. -T. (2022). Formation of Pixelated Elastic Films via Capillary Suction of Curable Elastomers in Templated Hele–Shaw Cells. Advanced Materials *34*, 2109682. 10.1002/adma.202109682.
- 21. Ilievski, F., Mazzeo, A.D., Shepherd, R.F., Chen, X., and Whitesides, G.M. (2011). Soft Robotics for Chemists. Angew. Chem. Int. Ed. *50*, 1890–1895. 10.1002/anie.201006464.
- 22. Kendre, S.V., Teran, G.T., Whiteside, L., Looney, T., Wheelock, R., Ghai, S., and Nemitz, M.P. (2022). Printable Flexible Robots for Remote Learning.
- 23. Cafferty, B.J., Campbell, V.E., Rothemund, P., Preston, D.J., Ainla, A., Fulleringer, N., Diaz, A.C., Fuentes, A.E., Sameoto, D., Lewis, J.A., et al. (2019). Fabricating 3D Structures by Combining 2D Printing and Relaxation of Strain. Adv. Mater. Technol. *4*, 1800299. 10.1002/admt.201800299.
- 24. Yirmibesoglu, O.D., Morrow, J., Walker, S., Gosrich, W., Canizares, R., Kim, H., Daalkhaijav, U., Fleming, C., Branyan, C., and Menguc, Y. (2018). Direct 3D printing of silicone elastomer soft robots and their performance comparison with molded counterparts. In 2018 IEEE International Conference on Soft Robotics (RoboSoft) (IEEE), pp. 295–302. 10.1109/ROBOSOFT.2018.8404935.
- 25. Rothemund, P., Ainla, A., Belding, L., Preston, D.J., Kurihara, S., Suo, Z., and Whitesides, G.M. (2018). A soft, bistable valve for autonomous control of soft actuators. Sci. Robot. *3*, eaar7986. 10.1126/scirobotics.aar7986.
- 26. Shepherd, R.F., Ilievski, F., Choi, W., Morin, S.A., Stokes, A.A., Mazzeo, A.D., Chen, X., Wang, M., and Whitesides, G.M. (2011). Multigait soft robot. Proceedings of the National Academy of Sciences *108*, 20400–20403. 10.1073/pnas.1116564108.
- 27. Kubo, M., Li, X., Kim, C., Hashimoto, M., Wiley, B.J., Ham, D., and Whitesides, G.M. (2010). Stretchable Microfluidic Radiofrequency Antennas. Adv. Mater. 22, 2749–2752. 10.1002/adma.200904201.



- 28. Mortimer, S., Ryan, A.J., and Stanford, J.L. (2001). Rheological Behavior and Gel-Point Determination for a Model Lewis Acid-Initiated Chain Growth Epoxy Resin. Macromolecules *34*, 2973–2980. 10.1021/ma001835x.
- 29. Nickerson, M.T., Patel, J., Heyd, D.V., Rousseau, D., and Paulson, A.T. (2006). Kinetic and mechanistic considerations in the gelation of genipin-crosslinked gelatin. International Journal of Biological Macromolecules 39, 298–302. 10.1016/j.ijbiomac.2006.04.010.
- 30. Harkous, A., Colomines, G., Leroy, E., Mousseau, P., and Deterre, R. (2016). The kinetic behavior of Liquid Silicone Rubber: A comparison between thermal and rheological approaches based on gel point determination. Reactive and Functional Polymers 101, 20–27. 10.1016/j.reactfunctpolym.2016.01.020.
- 31. Elsmore, M.T., and De Focatiis, D.S.A. (2021). Combined roles of temperature and humidity on cure of a silicone elastomer. Polymer Testing 93, 106967. 10.1016/j.polymertesting.2020.106967.
- 32. Tung, C.-Y.M., and Dynes, P.J. (1982). Relationship between viscoelastic properties and gelation in thermosetting systems. J. Appl. Polym. Sci. 27, 569–574. 10.1002/app.1982.070270220.
- 33. Lin-Gibson, S., Walls, H.J., Kennedy, S.B., and Welsh, E.R. (2003). Reaction kinetics and gel properties of blocked diisocyinate crosslinked chitosan hydrogels. Carbohydrate Polymers *54*, 193–199. 10.1016/S0144-8617(03)00159-0.
- 34. Bardelli, T., Marano, C., and Briatico Vangosa, F. (2021). Polydimethylsiloxane crosslinking kinetics: A systematic study on Sylgard184 comparing rheological and thermal approaches. J of Applied Polymer Sci *138*, 51013. 10.1002/app.51013.
- 35. Xie, J., Randolph, R., Simmons, G., Vinciguerra, M., Suri, S., Bonini, N., Root, A., Hull, P.V., and Mazzeo, A.D. (2019). Spreading of fast-curing, thermosetting silicones. Appl. Phys. Lett. *115*, 253701. 10.1063/1.5106388.
- 36. Luis, E., Pan, H.M., Sing, S.L., Bajpai, R., Song, J., and Yeong, W.Y. (2020). 3D Direct Printing of Silicone Meniscus Implant Using a Novel Heat-Cured Extrusion-Based Printer. Polymers *12*, 1031. 10.3390/polym12051031.
- 37. Vaicekauskaite, J., Mazurek, P., Vudayagiri, S., and Skov, A.L. (2020). Mapping the mechanical and electrical properties of commercial silicone elastomer formulations for stretchable transducers. J. Mater. Chem. C *8*, 1273–1279. 10.1039/C9TC05072H.



- 38. Park, S., Mondal, K., Treadway, R.M., Kumar, V., Ma, S., Holbery, J.D., and Dickey, M.D. (2018). Silicones for Stretchable and Durable Soft Devices: Beyond Sylgard-184. ACS Appl. Mater. Interfaces *10*, 11261–11268. 10.1021/acsami.7b18394.
- 39. Wolff, F., Kugler, C., and Münstedt, H. (2012). Time- and temperature-dependent crosslinking behaviour of a silicone resin. Rheol Acta *51*, 71–80. 10.1007/s00397-011-0585-7.
- 40. Yap, T.F., Liu, Z., Shveda, R.A., and Preston, D.J. (2020). A predictive model of the temperature-dependent inactivation of coronaviruses. Appl. Phys. Lett. *117*, 060601. 10.1063/5.0020782.
- 41. Yap, T.F., Hsu, J.C., Liu, Z., Rayavara, K., Tat, V., Tseng, C.-T.K., and Preston, D.J. (2021). Efficacy and self-similarity of SARS-CoV-2 thermal decontamination. Journal of Hazardous Materials, 127709. 10.1016/j.jhazmat.2021.127709.
- 42. Liu, P., Peng, L., Chen, J., Yang, B., Chen, Y., Luo, Z., Han, C.C., Huang, X., and Men, Y. (2022). Tensile Creep Failure of Isotactic Polypropylene under the Strain Criterion. Macromolecules *55*, 9663–9670. 10.1021/acs.macromol.2c01263.
- 43. Metselaar, R., and Oversluizen, G. (1984). The meyer-neldel rule in semiconductors. Journal of Solid State Chemistry *55*, 320–326. 10.1016/0022-4596(84)90284-6.
- 44. Takamure, N., Sun, X., Nagata, T., Ho-Baillie, A., Fukata, N., and McKenzie, D.R. (2022). Thermodynamic Interpretation of the Meyer-Neldel Rule Explains Temperature Dependence of Ion Diffusion in Silicate Glass. Phys. Rev. Lett. *129*, 175901. 10.1103/PhysRevLett.129.175901.
- 45. Bennett, C.A., Kistler, R.S., Nangia, K., Al-Ghawas, W., Al-Hajji, N., and Al-Jemaz, A. (2009). Observation of an Isokinetic Temperature and Compensation Effect for High-Temperature Crude Oil Fouling. Heat Transfer Engineering *30*, 794–804. 10.1080/01457630902751478.
- 46. Saseendran, S., Wysocki, M., and Varna, J. (2016). Evolution of viscoelastic behavior of a curing LY5052 epoxy resin in the glassy state. Advanced Manufacturing: Polymer & Composites Science 2, 74–82. 10.1080/20550340.2016.1236223.
- 47. O'Brien, D.J., Mather, P.T., and White, S.R. (2001). Viscoelastic Properties of an Epoxy Resin during Cure. j compos mater *35*, 883–904. 10.1177/002199801772662442.



- 48. Marechal, L., Balland, P., Lindenroth, L., Petrou, F., Kontovounisios, C., and Bello, F. (2021). Toward a Common Framework and Database of Materials for Soft Robotics. Soft Robotics 8, 284–297. 10.1089/soro.2019.0115.
- 49. Krpovic, S., Dam-Johansen, K., and Skov, A.L. (2021). Importance of Mullins effect in commercial silicone elastomer formulations for soft robotics. J Appl Polym Sci 138, 50380. 10.1002/app.50380.
- 50. Staudt, Y., Odenbreit, C., and Schneider, J. (2018). Failure behaviour of silicone adhesive in bonded connections with simple geometry. International Journal of Adhesion and Adhesives *82*, 126–138. 10.1016/j.ijadhadh.2017.12.015.
- 51. Zhao, Y.H., Guo, Y.Z., Wei, Q., Topping, T.D., Dangelewicz, A.M., Zhu, Y.T., Langdon, T.G., and Lavernia, E.J. (2009). Influence of specimen dimensions and strain measurement methods on tensile stress–strain curves. Materials Science and Engineering: A *525*, 68–77. 10.1016/j.msea.2009.06.031.
- 52. Brun, P.-T. (2022). Fluid-Mediated Fabrication of Complex Assemblies. JACS Au 2, 2417–2425. 10.1021/jacsau.2c00427.
- 53. Lee, C.-U., Chin, K.C.H., and Boydston, A.J. (2023). Additive Manufacturing by Heating at a Patterned Photothermal Interface. ACS Appl. Mater. Interfaces *15*, 16072–16078. 10.1021/acsami.3c00365.
- 54. Yee, D.W. (2023). A HAPPI solution: Photothermal additive manufacturing of unmodified thermoset resins. Matter *6*, 2488–2612. 10.1016/j.matt.2023.07.002.
- 55. Arun, N.D., Yang, H., Yao, L., and Feinberg, A.W. (2023). Nonplanar 3D Printing of Epoxy Using Freeform Reversible Embedding. Adv Materials Technologies, 2201542. 10.1002/admt.202201542.
- 56. Stang, M., Tashman, J., Shiwarski, D., Yang, H., Yao, L., and Feinberg, A. (2022). Embedded 3D Printing of Thermally-Cured Thermoset Elastomers and the Interdependence of Rheology and Machine Pathing. Adv Materials Technologies, 2200984. 10.1002/admt.202200984.
- 57. Walker, S., Lingle, E., Troxler, N., Wallin, T., Healy, K., Mengüç, Y., and Davidson, J.R. (2021). Predicting interfacial layer adhesion strength in 3D printable silicone. Additive Manufacturing *47*, 102320. 10.1016/j.addma.2021.102320.